



## Article

# Isolation and Characterization of Bioactive Compounds from *Saccharomonospora* sp. CMS18 and Their Antifungal Properties

Soohyun Um <sup>1,†</sup>, Hyeongju Jeong <sup>2,†</sup>, Ji-Eun Park <sup>3,4,†</sup>, Jeongwon Seo <sup>2</sup>, Sang Heon Jung <sup>5</sup>, Munhyung Bae <sup>5</sup>, Kyung-Tae Lee <sup>4,\*</sup>  and Kyuho Moon <sup>6,7,\*</sup> 

<sup>1</sup> College of Pharmacy, Yonsei University, Incheon 21983, Republic of Korea; soohyunum@yonsei.ac.kr

<sup>2</sup> Research Institute of Pharmaceutical Sciences, College of Pharmacy, Chonnam National University, Gwangju 61186, Republic of Korea; 217843@jnu.ac.kr (H.J.); jeongwon.0522@gmail.com (J.S.)

<sup>3</sup> Korea Research Institute for Veterinary Biologics, Iksan 54531, Republic of Korea; doraamong16@naver.com

<sup>4</sup> Korea Zoonosis Research Institute, Jeonbuk National University, Iksan 54531, Republic of Korea

<sup>5</sup> College of Pharmacy, Gachon University, Incheon 21936, Republic of Korea; fly6778@gachon.ac.kr (S.H.J.); baemoon89@gachon.ac.kr (M.B.)

<sup>6</sup> College of Pharmacy, Kyung Hee University, Seoul 02447, Republic of Korea

<sup>7</sup> Department of Biomedical and Pharmaceutical Sciences, Graduate School, Kyung Hee University, Seoul 02447, Republic of Korea

\* Correspondence: lee.kt@jbnu.ac.kr (K.-T.L.); kmoon@khu.ac.kr (K.M.)

† These authors contributed equally to this work.

**Abstract:** In this study, metagenomic analysis was employed to investigate the bacterial communities in the Muan tidal mudflat of the Republic of Korea. We used metagenomic analysis to identify the microbial community in tidal soil dominated by Proteobacteria. From this environment, the bacterial strain, *Saccharomonospora* sp. CMS18, was isolated and yielded two previously unknown compounds, penipaline D (3) and *N*-acetyl-dimethylallyltryptophan (4). The chemical structures of the isolated compounds along with 6-dimethylallyl-indole (1), 6-dimethylallyltryptophan (2), penipaline D (3), and *N*-acetyl-dimethylallyltryptophan (4) were structurally investigated using HR-ESI-MS and NMR spectroscopy. The isolated compound 6-dimethylallyl-indole (1) demonstrated broad-spectrum antifungal activity, with IC<sub>50</sub> value of 0.04 mM against *Candida glabrata* and 0.35 mM against both *Candida albicans* and *Cryptococcus neoformans*. Additionally, it exhibited additive interaction with caspofungin against *C. albicans*.

**Keywords:** tidal mudflat; structural determination; secondary metabolite; antifungal agent



**Citation:** Um, S.; Jeong, H.; Park, J.-E.; Seo, J.; Jung, S.H.; Bae, M.; Lee, K.-T.; Moon, K. Isolation and Characterization of Bioactive Compounds from *Saccharomonospora* sp. CMS18 and Their Antifungal Properties. *Mar. Drugs* **2024**, *22*, 539. <https://doi.org/10.3390/md22120539>

Academic Editor: Mostafa Rateb

Received: 26 October 2024

Revised: 26 November 2024

Accepted: 28 November 2024

Published: 30 November 2024



**Copyright:** © 2024 by the authors. Licensee MDPI, Basel, Switzerland. This article is an open access article distributed under the terms and conditions of the Creative Commons Attribution (CC BY) license (<https://creativecommons.org/licenses/by/4.0/>).

## 1. Introduction

The important roles played by tidal mudflats in the decomposition of organic matter and the cycling of nutrients have set them apart as dynamic coastal ecosystems [1]. These environments are home to a wide variety of microorganisms that actively participate in the decomposition of organic materials, thereby facilitating the recycling of vital nutrients [2,3]. Although the ecological roles of tidal flats have historically been the focus of research, they are also acknowledged as significant stores of bioactive natural products, particularly secondary metabolites produced by local microorganisms [4]. These substances have shown a great deal of promise for use in pharmaceutical applications; the development of new antibiotics and anticancer treatments is one example of this [5].

Actinomycetes are microorganisms that thrive in tidal mudflats and are distinguished by their abundant production of a variety of secondary metabolites [6,7]. For example, the well-known actinomycete *Streptomyces* is a source of several common antibiotics, including erythromycin, tetracycline, and streptomycin [8–10]. *Streptomyces* species are responsible for the synthesis of nystatin, an antifungal agent, and doxorubicin, an important antitumor agent [11,12]. Similarly, *Saccharomonospora* species also produce diverse bioactive compounds, many of which have been developed as therapeutic agents [13,14]. However, little

is known about the secondary metabolites produced by actinomycetes in tidal mudflat environments, especially in special places such as Korea's Muan tidal mudflat, which is regarded as one of the world's largest tidal flats [15].

Recent developments in metagenomic methodologies have provided a more profound understanding of the microbial diversity in these environments [16]. For instance, metagenomic sequencing has enabled a comprehensive definition of microbial communities inhabiting tidal flats and the identification of microbes that may be beneficial for the discovery of natural products [17,18]. In this study, the bioactive potential of actinomycetes, particularly those found in the Muan tidal mudflat, was investigated using a combination of traditional methods of natural product separation and metagenomic analysis.

Although the ecological importance of tidal mudflats has been widely acknowledged, research on the bioactive potential of these microbial communities is lacking. To address the gap in research on microbial bioactive compounds from tidal mudflats, we isolated *Saccharomonospora* sp. CMS18 from the Muan tidal mudflat. Three novel compounds were identified using advanced analytical techniques such as nuclear magnetic resonance (NMR) spectroscopy and high-resolution electrospray ionization mass spectrometry (HR-ESI-MS). Additionally, the biological activities of these compounds were assessed to highlight their potential therapeutic applications by assessing their antifungal efficacy against major invasive fungal pathogens.

## 2. Results and Discussion

### 2.1. Composition Analysis of Metagenomics Sequencing

By utilizing the genomic DNA isolated from the sediment, 424.8 bp read lengths (with a minimum of 148 and a maximum of 449) of the V3-V4 hypervariable sections of the bacterial 16S rRNA gene were amplified. Using the Illumina MiSeq platform, 55,298 amplicons were sequenced, and 41,765 quality-filtered reads were produced (low-quality amplicons = 3562, non-target amplicons = 78, and chimeric amplicons, 9893). The number of reads that could be classified as belonging to a specific species was 37,280 (89.3%), and 673 bacterial species were identified. Good's coverage, which reflects the database coverage rate of a sample, was calculated as the ratio of OTUs, excluding singletons, in the entire read. For the sediment, the values of alpha diversity, also known as species diversity, which exists in a certain place and in a specific sample, were 1, 631.8, 1520.5 for Chao1 and 1727. The sediment had a Shannon index value of 2.903, with a margin of error of 0.026. This value represented the number of species and the effect of evenness. The phylogenetic diversity of the mud sample was found to be 1920 after calculating the shortest distances between the nodes of the system diagram. The discovered OTUs were categorized into the following groups: 32 phyla (41,765 OTUs), 74 classes, 142 orders, 249 families, 551 genera, and 783 species. Proteobacteria, the dominant taxon, were identified in 96.6% of the total 32 phyla, including Bacteroidetes (1.1%), Acidobacteria (0.34%), Chloroflexi (0.3%), and Actinobacteria (0.2%). Gammaproteobacteria was the most prevalent phylum within the phylum Proteobacteria, accounting for 75.7% of all readings. This was followed by Deltaproteobacteria and Betaproteobacteria, which accounted for 7.0% and 6.6% of all reads, respectively, at the class level. At the order level, Methylococcales comprised 58.9% of the population. This was followed by the Methylophilales (6.5%) and Oceanospirillales (14.4%) (Figure 1).

Metagenomic analysis indicated that Actinobacteria, which encompasses genera such as *Streptomyces* and *Saccharomonospora*, constituted only 0.2% of the overall bacterial community in the sediment. The low proportion of Actinobacteria may be attributed to limitations of metagenomic sequencing, which often fails to capture slow-growing or low-abundance microorganisms in environmental samples. Additionally, Actinobacteria may require particular growth conditions, and their metabolic activity may be inhibited under specific environmental conditions, rendering them less detectable via metagenomic techniques. Despite the low abundance of Actinobacteria observed in the metagenomic analysis, the isolation of *Saccharomonospora* sp. CMS18, using traditional culturing techniques, highlights

the importance of integrating both cultivation-dependent and cultivation-independent methods. This discrepancy underscores the limitations of metagenomics in identifying bioactive microorganisms and emphasizes the need for culturing techniques to fully assess the metabolic potential of tidal flat microbial communities.

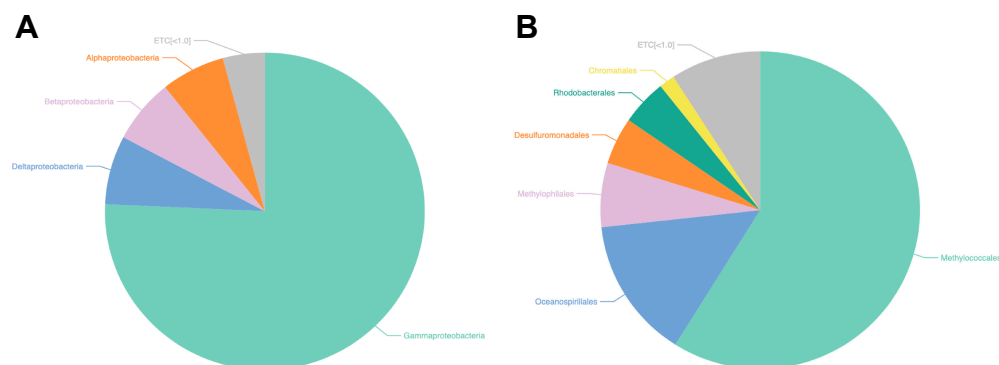


**Figure 1.** Metagenomics targeted bacteria taxon of the mud sample. The data show Microbiome Taxonomic Profile (MTP) for the mud sample at the level of (A) class and (B) order.

## 2.2. Structural Elucidation

6-Dimethylallyl-indole (**1**) and 6-dimethylallyltryptophan (**2**) were isolated from actinomycete *Saccharomonospora* sp. CMS18 and its chemical structure were determined by liquid LC-MS, high-resolution electrospray ionization mass spectrometry (HR-ESI-MS), and nuclear magnetic resonance (NMR) analysis. Compounds **1** and **2** were obtained as colorless and yellow oils, respectively, and their molecular formulae were determined to be  $C_{13}H_{15}N$  and  $C_{16}H_{20}N_2O_2$  by HR-ESI-MS ( $m/z$  186.1277  $[M + H]^+$  calculated for  $C_{13}H_{15}N$   $m/z$  186.1277  $[M + H]^+$  and  $m/z$  273.1604  $[M + H]^+$  calculated for  $C_{16}H_{21}N_2O_2$ ,  $m/z$  273.1597  $[M + H]^+$ ) together with  $^1H$  and  $^{13}C$  NMR data (Tables 1 and 2). The chemical structures of **1** and **2** were confirmed using 1D ( $^1H$  and  $^{13}C$ ) and 2D (COSY, HSQC, and HMBC) NMR spectroscopy, with the spectra recorded in methanol- $d_4$  ( $CD_3OD-d_4$ ). The chemical structures of **1** and **2** were identified as 6-dimethylallyl-indole and 6-dimethylallyltryptophan by comparing the NMR data with the literature (Figure 2) [19–21].

**Table 1.**  $^1H$  and  $^{13}C$  NMR spectroscopic data of 6-dimethylallyl-indole (**1**) in  $CD_3OD-d_4$ .

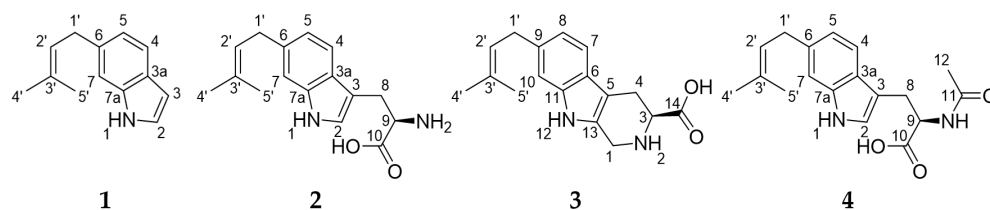
Position	6-Dimethylallyl-indole ( <b>1</b> )	
	$\delta_C$ , Type	$\delta_H$ , Mult (J in Hz)
2	124.9, CH	7.14, d (3.0)
3	102.0, CH	6.36, d (3.0)
3a	127.6, C	-
4	120.9, CH	7.42, d (8.0)
5	121.1, CH	6.83, d (8.0)
6	136.0, C	-
7	111.2, CH	7.16, s
7a	138.1, C	-
1'	3.52, CH <sub>2</sub>	3.41, d (7.5)
2'	125.6, CH	5.38, t (7.5)
3'	132.3, C	-
4'	17.9, CH <sub>3</sub>	1.76, s
5'	25.9, CH <sub>3</sub>	1.76, s

$^1H$  and  $^{13}C$  NMR data were recorded at 700 and 175 MHz.

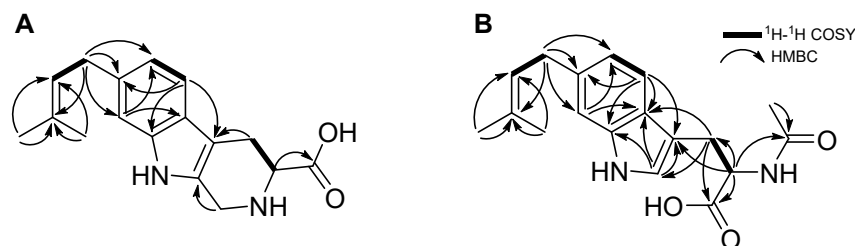
**Table 2.**  $^1\text{H}$  and  $^{13}\text{C}$  NMR spectroscopic data of 6-dimethylallyl-L-tryptophan (**2**) in  $\text{CD}_3\text{OD}-d_4$ .

Position	6-Dimethylallyl-L-tryptophan ( <b>2</b> )	
	$\delta_{\text{C}}$ , Type	$\delta_{\text{H}}$ , Mult (J in Hz)
2	124.9, CH	7.14, s
3	108.4, C	-
3a	126.5, C	-
4	118.9, CH	7.52, d (8.0)
5	121.4, CH	6.89, d (8.0)
6	136.9, C	-
7	111.7, CH	7.17, s
7a	138.8, C	-
8	28.0, $\text{CH}_2$	3.49, dd (15.0, 5.0) 3.23, dd (15.0, 8.0)
9	55.5, CH	4.07, dd (8.0, 5.0)
10	173.4, C	-
1'	35.5, $\text{CH}_2$	3.41, d (7.5)
2'	125.4, CH	5.35, t (7.5)
3'	132.6, C	-
4'	17.9, $\text{CH}_3$	1.74, s
5'	25.9, $\text{CH}_3$	1.74, s

$^1\text{H}$  and  $^{13}\text{C}$  NMR data were recorded at 600 and 150 MHz.

**Figure 2.** Structures of 6-dimethylallyl-indole (**1**), 6-dimethylallyltryptophan (**2**), penipaline D (**3**), and *N*-Acetyl-6-dimethylallyltryptophan (**4**).

Penipaline D (**3**) was isolated as a yellow oil, and its molecular formula was determined to be  $\text{C}_{17}\text{H}_{20}\text{N}_2\text{O}_2$  based on HR-ESI-MS ( $m/z$  285.1588  $[\text{M} + \text{H}]^+$ , calculated for  $\text{C}_{17}\text{H}_{21}\text{N}_2\text{O}_2$ ,  $m/z$  285.1597  $[\text{M} + \text{H}]^+$ ) in combination with  $^1\text{H}$  and  $^{13}\text{C}$  NMR spectroscopic data (Table 3). A comparison of the NMR data of **3** with those of **2** and **4** indicated that the structures of the compounds were very similar in the dimethylallyl group and indole moiety, except for the cyclized tryptophan in **3**. The HMBC correlations from  $\text{H}_{2-4}$  ( $\delta_{\text{H}}$  3.41 and 3.03) to C-5 ( $\delta_{\text{C}}$  107.7); from  $\text{H}_{2-1}$  ( $\delta_{\text{H}}$  4.39) to C-13 ( $\delta_{\text{C}}$  126.1); and from H-3 ( $\delta_{\text{H}}$  3.94) to C-14 ( $\delta_{\text{C}}$  173.9) indicated **3** has cyclomethyltryptophan instead of the tryptophan (Figures 2 and 3). Thus, the structure of **3** was determined as a  $\beta$ -carboline derivative, named penipaline D (**3**) [22].

**Figure 3.** Key  $^1\text{H}$ - $^1\text{H}$  COSY and HMBC correlations of (A) **3** and (B) **4**.

**Table 3.**  $^1\text{H}$  and  $^{13}\text{C}$  NMR spectroscopic data of penipaline D (3) in  $\text{CD}_3\text{OD}-d_4$ .

Position	Penipaline D (3) <sup>a</sup>	
	$\delta_{\text{C}}$ , Type	$\delta_{\text{H}}$ , Mult (J in Hz)
1	41.9, CH <sub>2</sub>	4.39, d (6.5)
3	59.0, CH	3.94, m
4	24.2, CH <sub>2</sub>	3.41, m
5	107.7, C	3.03, m
6	125.8, C	-
7	118.8, CH	7.36, d (8.0)
8	121.5, CH	6.89, d (8.0)
9	137.3, C	-
10	111.4, CH	7.11, s
11	138.9, C	-
13	126.1, C	-
14	173.9, C	-
1'	35.5, CH <sub>2</sub>	3.41, m
2'	125.3, CH	5.36, t (7.5)
3'	132.7, C	-
4'	17.9, CH <sub>3</sub>	1.75, s
5'	25.9, CH <sub>3</sub>	1.75, s

<sup>a</sup>  $^1\text{H}$  and  $^{13}\text{C}$  NMR data were recorded at 700 and 175 MHz.

*N*-Acetyl-6-dimethylallyl-L-tryptophan (**4**) was obtained as a colorless oil, and its molecular formula was assigned as  $\text{C}_{18}\text{H}_{22}\text{N}_2\text{O}_3$  by HR-ESI-MS ( $m/z$  315.1713 [ $\text{M} + \text{H}$ ]<sup>+</sup>, calculated for  $\text{C}_{18}\text{H}_{23}\text{N}_2\text{O}_3$ ,  $m/z$  315.1703 [ $\text{M} + \text{H}$ ]<sup>+</sup>) in combination with  $^1\text{H}$  and  $^{13}\text{C}$  NMR data (Table 4). The chemical structure of **4** was elucidated using the 1D and 2D NMR spectra acquired using methanol- $d_4$  ( $\text{CD}_3\text{OD}-d_4$ ). The  $^1\text{H}$  NMR spectrum of compound **4** reveals the following: an alpha proton at  $\delta_{\text{H}}$  4.70; beta protons at  $\delta_{\text{H}}$  3.31 and 3.12 of dimethylallyl tryptophan; indole ring protons at  $\delta_{\text{H}}$  7.44, 7.11, 7.01, and 6.85; and a dimethylallyl group with protons at  $\delta_{\text{H}}$  5.36, 3.40 (2H), and 1.75 (6H). The  $^{13}\text{C}$  NMR and HSQC spectra indicated that compound **4** bears 10 olefinic carbons ( $\delta_{\text{C}}$  138.5, 136.3, 132.4, 127.1, 125.6, 123.8, 120.9, 119.0, 111.4, and 110.9), 2 carbonyl groups ( $\delta_{\text{C}}$  175.3 and 173.2), and 3 methyl groups ( $\delta_{\text{C}}$  25.9, 22.4, and 17.9). The COSY correlations between H-4 ( $\delta_{\text{H}}$  7.44) and H-5 ( $\delta_{\text{H}}$  6.85) and the HMBC correlations from H-4 to C-3 ( $\delta_{\text{C}}$  110.9), C-3a ( $\delta_{\text{C}}$  127.1), C-6 ( $\delta_{\text{C}}$  136.3), and C-7a ( $\delta_{\text{C}}$  138.5); from H-7 ( $\delta_{\text{H}}$  7.11) to C-3a and C-5 ( $\delta_{\text{C}}$  120.9); and from H-2 ( $\delta_{\text{H}}$  7.01) to C-3, C-3a and C-7a established the indole ring of **4**. The COSY correlation of H-9 ( $\delta_{\text{H}}$  4.70) with H<sub>2</sub>-8 ( $\delta_{\text{H}}$  3.31 and 3.12) and the HMBC correlations from H<sub>2</sub>-8 to C-10 ( $\delta_{\text{C}}$  175.3), C-9 ( $\delta_{\text{C}}$  54.8), C-3, C-3a, and C-2 ( $\delta_{\text{C}}$  123.8) indicated that **4** bears the tryptophan moiety. The characteristic signals for a dimethylallyl moiety were observed by the COSY correlation with H-1' ( $\delta_{\text{H}}$  3.40) to H-2' ( $\delta_{\text{H}}$  5.36) and the HMBC correlations from H-4' ( $\delta_{\text{H}}$  1.75) and H-5' ( $\delta_{\text{H}}$  1.75) to C-2' ( $\delta_{\text{C}}$  125.6) and from H-4', H-5', and H-1' to C-3' ( $\delta_{\text{C}}$  132.4). Lastly, the dimethylallyl group and tryptophan were linked by the HMBC correlations from H-1' to C-5, C-6, and C-7 ( $\delta_{\text{C}}$  111.4). An *N*-Acetyl group was confirmed by signals for carbonyl carbon ( $\delta_{\text{C}}$  173.2) and a methyl group ( $\delta_{\text{H}}$  1.90 and  $\delta_{\text{C}}$  22.4). The HMBC correlations from H-9 and H-12 ( $\delta_{\text{H}}$  1.90) to C-11 ( $\delta_{\text{C}}$  173.2) constructed the connections between these partial structures of **4** (Figures 2 and 3). Thus, the planar structure of **4** was determined as *N*-Acetyl-6-dimethylallyltryptophan. The absolute configurations of the compounds were assigned by comparing experimental circular dichroism (CD) and calculated CD spectra (Figures S25 and S26) and the optical rotation comparison with the reference [19,22].

**Table 4.** <sup>1</sup>H and <sup>13</sup>C NMR spectroscopic data of *N*-acetyl-6-dimethylallyl-L-tryptophan (**4**) in CD<sub>3</sub>OD-*d*<sub>4</sub>.

Position	<i>N</i> -Acetyl-6-dimethylallyl-L-tryptophan ( <b>4</b> ) <sup>c</sup>	
	δ <sub>C</sub> , Type	δ <sub>H</sub> , Mult (J in Hz)
2	123.8, CH	7.01, s
3	110.9, C	4.70, dd (8.0, 5.0)
3a	127.1, C	3.31, m
4	119.0, CH	7.44, d (8.0)
5	120.9, CH	6.85, d (8.0)
6	136.3, C	-
7	111.4, CH	7.11, s
7a	138.5, C	-
8	28.6, CH <sub>2</sub>	3.31, m
9	54.8, CH	3.12, dd (15.0, 8.0)
10	175.3, C	4.70, dd (8.0, 5.0)
11	173.2, C	-
12	22.4, CH <sub>3</sub>	-
1'	22.4, CH <sub>3</sub>	1.90, s
2'	123.8, CH	7.01, s
3'	173.2, C	-
4'	22.4, CH <sub>3</sub>	1.90, s
5'	35.5, CH <sub>2</sub>	3.40, d (7.5)
5'	125.6, CH	5.36, t (7.5)

<sup>c</sup> <sup>1</sup>H and <sup>13</sup>C NMR data were recorded at 900 and 225 MHz.

### 2.3. Assessment of Antifungal Efficacy

To evaluate the antifungal efficacy, we performed a minimum inhibitory concentration (MIC) assay to assess the effectiveness of the compounds against major invasive fungal pathogens, including *Candida albicans*, *C. glabrata*, *C. auris*, and *Cryptococcus neoformans*. Notably, compound **1** demonstrated broad-spectrum inhibitory efficacy with an IC<sub>50</sub> of 0.043 mM against *C. glabrata* and 0.35 mM against *C. albicans*, *C. auris*, and *C. neoformans*. In contrast, compounds **2**, **3**, and **4** did not exhibit significant inhibitory effects on any of the tested fungal pathogens (Table 5).

**Table 5.** Antifungal activity of the compounds against human fungal pathogens.

Cpd.	<i>C. albicans</i>			<i>C. glabrata</i>			<i>C. auris</i>			<i>C. neoformans</i>		
	IC <sub>20</sub>	IC <sub>50</sub>	IC <sub>90</sub>	IC <sub>20</sub>	IC <sub>50</sub>	IC <sub>90</sub>	IC <sub>20</sub>	IC <sub>50</sub>	IC <sub>90</sub>	IC <sub>20</sub>	IC <sub>50</sub>	IC <sub>90</sub>
1	0.17	0.35	>0.69	0.04	0.04	>0.69	0.17	0.35	>0.69	0.17	0.35	>0.69
2	0.47	>0.47	>0.47	0.12	>0.47	>0.47	>0.47	>0.47	>0.47	0.47	>0.47	>0.47
3	>0.45	>0.45	>0.45	0.12	0.45	>0.45	0.45	>0.45	>0.45	0.45	>0.45	>0.45
4	>0.41	>0.41	>0.41	0.10	>0.41	>0.41	>0.41	>0.41	>0.41	>0.41	>0.41	>0.41

IC<sub>20</sub>, IC<sub>50</sub>, and IC<sub>90</sub> refer to 20%, 50%, and 90% inhibitory concentrations (mM), respectively.

To further understand the molecular impact of these compounds, we examined the changes in gene expression after treatment. Drug efflux pumps, such as *CDR1* and *CDR2*, which are commonly upregulated in response to antifungal agents, were analyzed [23]. Our results revealed that compound **1** significantly induced *CDR2* expression, while compound **3** led to a significant increase in *CDR1* expression (Figure 4A). Additionally, with respect to cell wall integrity, compound **3** induced the expression of *CRZ1*, a transcription factor in the calcineurin signaling pathway (Figure 4B). Interestingly, compound **1** treatment led to the repression of *ECE1*, the gene responsible for producing candidalysin, a key virulence factor in *C. albicans* (Figure 4C). This gene repression suggested that compound **1** could be a potential therapeutic agent for targeting virulence mechanisms. Based on these findings, we selected compounds **1** and **3** for further analysis because of their drug-like effects on *C. albicans*.

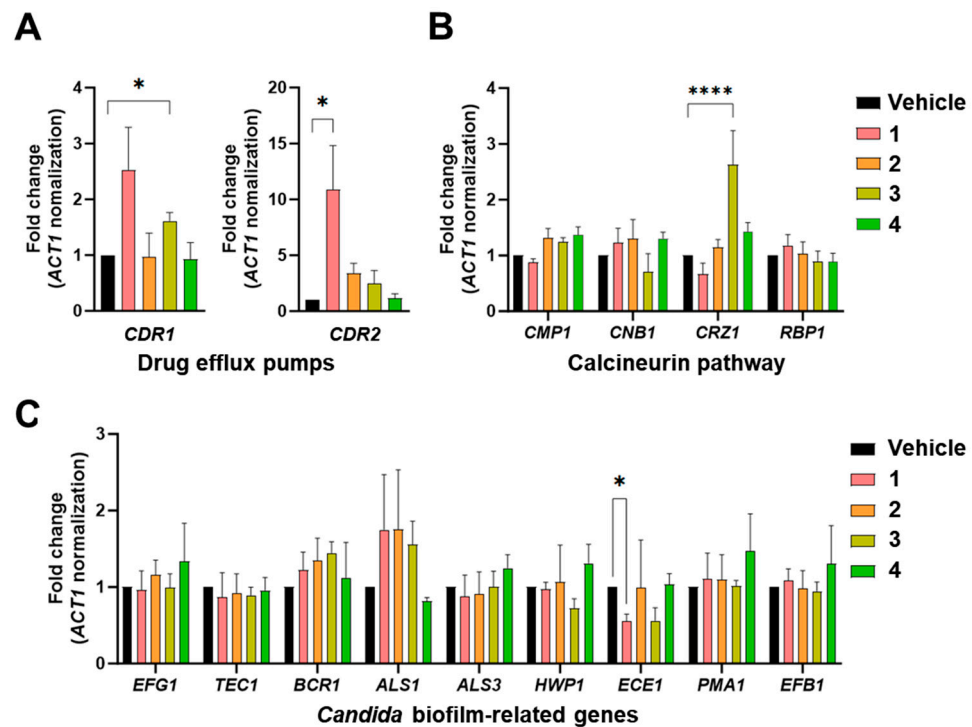


**Figure 4.** Gene expression regulated by compounds in *Candida albicans*. *Candida albicans* cells in early exponential growth phase were cultured in yeast-extracted peptone medium and treated with drugs at the  $IC_{50}$  level. Total RNA was extracted, converted into cDNA, and subsequently analyzed using quantitative PCR. (A) Genes encoding drug efflux pumps. (B) Genes involved in calcineurin signaling pathway. (C) Genes associated with biofilm formation. The  $p$  values from the multiple comparisons in ANOVA analysis are as follows: \*,  $p < 0.05$ ; \*\*\*\*,  $p < 0.0001$ .

#### 2.4. Optimization of Antifungal Potency

We examined and compared the inhibition of fungal growth and biofilm formation by compounds **1** and **3**. The growth inhibition efficacy of compound **1** was closely correlated with biofilm reduction. In *C. albicans* and *C. auris*, which experienced up to 50% growth inhibition by compound **1**, biofilm production was reduced by up to 10%. Compound **3** inhibited the growth of *C. glabrata* by up to 5% and displayed a similar pattern of biofilm inhibition. Interestingly, despite the lower efficacy of compound **3** in growth inhibition, *C. albicans* biofilms were reduced by up to 10% and *C. auris* biofilms by up to 6% (Figure 5A). Compound **1** exhibited broad-spectrum growth inhibition against fungal pathogens such as *C. albicans*, *C. glabrata*, *C. auris*, and *C. neoformans*, whereas compound **3** effectively inhibited biofilm formation in *C. albicans* and *C. auris*.

Subsequently, we investigated the potential synergistic effects of compound **1** in combination with standard antifungal drugs to enhance its growth inhibitory efficacy against *C. albicans* (Figure 5B). The combination of compound **1** with amphotericin B showed no synergistic effect (FIC score = 2.00; no interaction). However, caspofungin exhibited an additive interaction with the two agents (FIC score = 0.56). These findings suggest that, although compound **1** exhibits broad-spectrum antifungal activity, particularly against *C. albicans*, its combination with caspofungin offers an additive therapeutic effect, indicating its potential for enhanced treatment strategies targeting fungal pathogens.

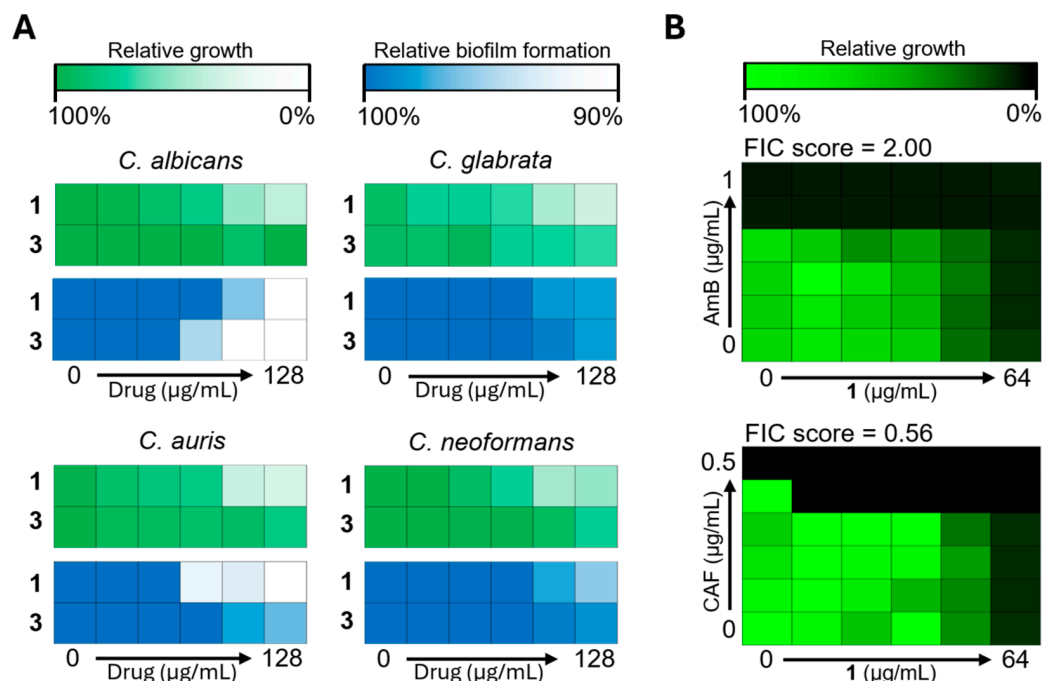


**Figure 5.** Evaluation of biofilm inhibition efficacy and drug synergy in *Candida albicans*. (A) Fungal growth following treatment with compounds **1** and **3** was measured by absorbance at OD 600 nm. After washing, biofilm formation was stained with crystal violet, and the residual dye was destained and measured by absorbance at OD 590 nm. (B) Compound **1** was tested in combination with amphotericin B (AmB) and caspofungin (CAF) using a checkerboard assay to assess drug synergy.

### 3. Materials and Methods

#### 3.1. General Experimental Procedures

General rotations were measured using a Jasco P-2000 polarimeter (Tokyo, Japan) with a 1.0 cm cell. UV spectra and LC/MS data were recorded using an Agilent G6125B MSD system coupled with an Agilent Technologies 1260 series Infinity II LC system (Agilent Technologies, Santa Clara, CA, USA) using a reversed-phase Phenomenex Luna C18 column (Phenomenex, Torrance, CA, USA, 100 × 4.6 mm, 5 µm). CD spectra were obtained with a 1 mm cell using Chirascan Plus (Applied Photophysics, Leatherhead, Surrey, UK). Infrared (IR) spectra were acquired using a Spectrum 3 Fourier Transform Infrared Spectrometer (PerkinElmer, Waltham, MA, USA). High-resolution electrospray ionization mass spectra (HR-ESI-MS) were obtained using an Agilent Technologies 1290 series HPLC coupled with an Agilent 6530 iFunnel Q-TOF LC/MS system (Agilent Technologies, Santa Clara, CA, USA). Moreover,  $^1\text{H}$ ,  $^{13}\text{C}$ , and 2D NMR spectra were recorded on an Agilent VNMR 600 MHz spectrometer (Agilent Technologies, Santa Clara, CA, USA) at the Korea Basic Science Institute (KBSI) in Gwangju and a Bruker Advance III 700 MHz spectrometer (Bruker, Billerica, MA, USA) and a Bruker Advance II 900 MHz spectrometer (Bruker, Billerica, MA, USA) at the KBSI in Ochang. HPLC purification was performed on a Waters system (Waters, Milford, MA, USA) 1525 binary HPLC pump and 996 photodiode array detector with a YMC (YMC, Kyoto, Japan) Pack-ODS-A-C18 column (250 × 10 mm, 5 µm).

#### 3.2. Collection of Tidal Flat Samples and Isolation of Bacterial Strain

Tidal mudflat sediment samples were collected in Muan, Republic of Korea, in August 2020. Mixtures of dried samples and 4 mL of sterilized water (2 g each) were heated to 55 °C and sonicated. The mixtures were spread on A1 medium (agar 18 g, sea salt 33 g, and 1 L of distilled water), Chitin medium (chitin 4 g,  $\text{K}_2\text{HPO}_4$  0.75 g,  $\text{MgSO}_4 \cdot 7\text{H}_2\text{O}$  0.5 g,  $\text{KH}_2\text{PO}_4$  3.5 g,  $\text{FeSO}_4 \cdot 7\text{H}_2\text{O}$  10 mg,  $\text{MnCl}_2 \cdot 7\text{H}_2\text{O}$  10 mg,  $\text{ZnSO}_4 \cdot 7\text{H}_2\text{O}$  10 mg, agar 18 g, sea salt 33 g, and 1 L of distilled water), SIM medium (casein 0.4 g, starch 1 g,  $\text{KNO}_3$  0.5 g,  $\text{K}_2\text{HPO}_4$  0.2 g,  $\text{MgSO}_4 \cdot 7\text{H}_2\text{O}$  0.1 g,  $\text{CaCO}_3$  0.1 g, agar 18 g, sea salt 33 g, and 1 L of distilled



water), TWYE medium (K<sub>2</sub>HPO<sub>4</sub> 0.5 g, yeast extract 0.25 g, agar 18 g, sea salt 33 g, and 1 L of distilled water), Kuster medium (glycerol 10 mL, casein 0.3 g, KNO<sub>3</sub> 3 g, K<sub>2</sub>HPO<sub>4</sub> 2 g, NaCl 2 g, MgSO<sub>4</sub>·7H<sub>2</sub>O 0.05 g, CaCO<sub>3</sub> 20 mg, FeSO<sub>4</sub> 10 mg, agar 18 g, sea salt 33 g, and 1 L of distilled water) with cycloheximide (50 mg/L), and nalidixic acid (20 mg/L). The CMS18 strain was isolated from the TWYE agar medium and identified as *Saccharomonospora* sp. (99.9% identical to *Saccharomonospora azurea*) based on 16S rDNA gene sequence analysis (GenBank accession number AGIU02000033.1).

### 3.3. DNA Extraction for Metagenomics

DNA was prepared using the FastDNA<sup>®</sup> Spin Kit for soil (MP Bio-medicals, Irvine, CA, USA), and its concentration was determined using an Epoch<sup>™</sup> Spectrometer (BioTek, Winooski, VT, USA). The hypervariable regions V3 and V4 of the 16S rRNA gene of bacteria were amplified by using the primer pair 341F [5'-TCGTCGGCAGCGTC-AGATGTGTATAAGAGACAG-CCTACGGGNGGCWGCAG-3', 50mer] and 805R [5'-GTCTCGTGGGCTCGG-AGATGTGTATAAGAGACAG-GACTACHVGGGTATCTAATCC-3', 55mer] followed by Illumina's 16S Metagenomics Protocol (Illumina, Inc., San Diego, CA, USA) for the first amplicon PCR. The second PCR (index PCR) was conducted with the forward index i5 [AATGATACGGCACCACCGAGATCTACAC-XXXXXX-TCGTCGGCAGCGTC, composition: left-i5 (XXXXXXX)-right, 51mer] and reverse index i7 [CAAGCAGAAGACGGCATA CGAGAT-GTCTCGTGGGCTCGG, composition: left-i5 (XXXXXXX)-right, 47mer]. The PCR reagents included 10× buffer (2.5 L), dNTP (2.5 L), forward primer (10 pmol/L, 1 L), and reverse primer (10 pmol/L, 1 L). Taq polymerase (TaKaRa Ex Taq DNA polymerase, 1000 U), DNA (2 L), and D.W. (15.75 L) were used. The total volume of the PCR reaction was 25 µL. The Quanti-iT PicoGreen dsDNA Assay Kit provided by Invitrogen (Invitrogen, Carlsbad, CA, USA) in conjunction with the Agilent 2100 Bioanalyzer System was utilized in order to ascertain both the quantity and quality of a single library (Agilent Technologies, Santa Clara, CA, USA). A MiSeq<sup>®</sup> Reagent Kit version 2 was used to perform paired-end sequencing on the samples (500 cycles; Illumina, Inc., San Diego, CA, USA).

### 3.4. Bioinformatics Analysis

To determine Q-values by sequence, sequences that could potentially be misinterpreted as “new species” based on their Q-value were eliminated. Trimmomatic software (version 0.40) was used to analyze next-generation sequencing (NGS) data produced by Illumina, and the researchers independently developed the code to evaluate other NGS data. The Pandaseq software (version 2.11) was implemented for bioinformatics purposes; however, this was not the case for PacBio single-end reads or CCS data [24]. In conjunction with in-house algorithms, the CJ Bioscience workflow was employed to eliminate the 16S rRNA PCR primer sequences using the in-house EzBioCloud 16S rRNA database. The annealing procedure generated these primer regions; therefore, their elimination was necessary. The 16S rRNA sequences were matched using various reference databases. This contributes to a reduction in computational labor and an improvement in accuracy. For additional analysis, both in-house methods and the HMMER program were used. Approximately 0.5% of raw NGS data contained sequencing errors that may have occurred at any time. Since the same gene was sequenced several times during the NGS studies, these mistakes could be corrected by applying suitable models. To determine the identity of each sequence, the pipeline relied on the tried-and-true identification techniques stored in EzBioCloud. The first phase of this two-part technique involved searching reference databases using the USEARCH program. The second step was to calculate similarity using a robust pairwise alignment. Query sequences were considered to be at the species level if they were at least 97% similar to the reference sequences in EzBioCloud. Lower cutoffs for sequence similarity were employed for higher taxonomic levels, such as genera. \*x = the degree to which the sequence in question is comparable to that of a reference sequence: species (×97%), genus (97 > ×94.5%), family (94.5 > ×86.5%), order (86.5 > ×82%), class (82 > ×78.5%), and phylum (78.5 > ×75%). In this investigation, the cutoff values deter-

mined by Yarza et al. were taken into consideration [25]. However, during the process of detecting chimeric sequences, sequences with less than 97% similarity in the identification phase were identified. Because this sequence had already been identified at the species level, it was eliminated as the detection target. Operational taxonomic units (OTUs) are arbitrary classification units frequently referred to as a “species” in microbial community research. OTUs are operational taxonomic units.

### 3.5. Taxonomic Analysis and Alpha- and Beta-Diversity

Each sequence was partitioned into multiple operational OTUs using various methods and computer programs. Sequences that shared less than 97% similarity were defined as a species, and each was assigned an OTU, with the exception of chimeras. Using the CD-hit and UCLUST algorithms, cluster analysis was conducted on sequences that were less than 97% identical, and an OTU was established for each cluster that emerged. The final OTU information was obtained by integrating the OTUs discovered in steps one and two. The OTU produced as a single sequence was omitted from the diversity analysis because its existence led to a greater increase in the diversity index than the real value. In addition to the Shannon and Simpson statistics, various indices of species abundance and evenness were included to calculate alpha diversity.

### 3.6. Large-Scale Cultivation and Extraction

The CMS18 strain was cultured in 50 mL of YEME medium (glucose 10 g, yeast extract 3 g, malt extract 3 g, peptone 5 g, soybean extract 2 g, sea salt 33 g, and 1 L of distilled water) in a 125 mL flask on a rotary shaker for 3 days at 30 °C and 190 rpm. For the first scale-up, a 3.5 mL aliquot of the broth culture was used to inoculate 150 mL of YEME medium in a 500 mL flask, which was then cultured under the same conditions. Twenty milliliters of the culture was transferred to 1 L of YEME medium in 2.5 L ultra-yield flasks (10 each 1 L, total volume 10 L) for 5 days under the same fermentation conditions. The CMS18 strain was isolated from the whole culture (in EtOAc) using 15 L of ethyl acetate. The EtOAc and water layers were separated, and the remaining water in the EtOAc layer was eliminated by adding anhydrous sodium sulfate. The EtOAc extract was concentrated under vacuum to obtain a solid substance.

### 3.7. Isolation and Purification of Compounds

The CMS18 strain dried material was fractionated over a C<sub>18</sub> reversed-phase column (YMC ODS-A C<sub>18</sub>, 50 µm silica gel) using a step gradient solvent system (20, 40, 60, 80, and 100% MeOH/H<sub>2</sub>O). Compound **1** was detected in the CMS18 80% MeOH/H<sub>2</sub>O fraction, and compounds **2**, **3**, and **4** were detected in the CMS18 60% MeOH/H<sub>2</sub>O fraction. Each fraction was filtered through a syringe filter (Advantec, Tokyo, Japan, HP020AN) and subjected to semi-preparative reversed-phase HPLC at a flow rate of 2 mL/min using a linear gradient and an isocratic solvent system. The CMS18 80% fraction was purified using isocratic 70% CH<sub>3</sub>CN/H<sub>2</sub>O, and **1** was eluted after 24.6 min. The CMS18 60% fraction was purified using a linear gradient of 25% to 40% CH<sub>3</sub>CN/H<sub>2</sub>O for 40 min (YMC ODS-A-C18:250 × 10 mm, 5 µm, UV detection at 254 nm). Under these HPLC conditions, **2** was eluted at 17 min, **3** at 30, and **4** at 33 min. Finally, the samples were purified to yield the pure compounds **1** (2.1 mg), **2** (10 mg), **3** (1.7 mg), and **4** (2 mg).

*6-dimethylallyl-indole (1)*: colorless oil, UV (MeOH)  $\lambda_{\max}$  (log  $\epsilon$ ) 225 (3.78) nm, 280 (3.44) nm; IR (ATR)  $\nu_{\max}$  3116, 3050, 1534, 1350 cm<sup>-1</sup>; and <sup>1</sup>H and <sup>13</sup>C NMR data (Table 1), HR-ESI-MS  $m/z$  186.1277 [M + H]<sup>+</sup> (calculated for C<sub>13</sub>H<sub>16</sub>N, 186.1277 [M + H]<sup>+</sup>).

*6-dimethylallyl-L-tryptophan (2)*: yellow oil,  $[\alpha]_{25}^D + 2.49$  (c 0.1, MeOH); UV (MeOH)  $\lambda_{\max}$  (log  $\epsilon$ ) 225 (3.98) nm, 280 (3.40) nm; IR (ATR)  $\nu_{\max}$  3174, 3059, 1804, 1268 cm<sup>-1</sup>; CD (c 0.01, MeOH) ( $\Delta\epsilon$ ) 228 (2.65), 260 (−0.73); and <sup>1</sup>H and <sup>13</sup>C NMR data (Table 2), HR-ESI-MS  $m/z$  273.1604 [M + H]<sup>+</sup> (calculated for C<sub>16</sub>H<sub>21</sub>N<sub>2</sub>O<sub>2</sub>, 273.1597 [M + H]<sup>+</sup>).

*penipaline D (3)*: yellow oil,  $[\alpha]_{25}^D - 1.15$  (c 0.1, MeOH); UV (MeOH)  $\lambda_{\max}$  (log  $\epsilon$ ) 225 (4.02) nm, 270 (3.25) nm; IR (ATR)  $\nu_{\max}$  3224, 3049, 2904, 1287 cm<sup>-1</sup>; and <sup>1</sup>H and <sup>13</sup>C

NMR data (Table 3), HR-ESI-MS  $m/z$  285.1588  $[M + H]^+$  (calculated for  $C_{17}H_{21}N_2O_2$ ,  $m/z$  285.1597  $[M + H]^+$ ).

*N*-acetyl-6-dimethylallyl-L-tryptophan (4): colorless oil,  $[\alpha]_{25}^D +2.82$  (c 0.1, MeOH); UV (MeOH)  $\lambda_{max}$  (log  $\epsilon$ ) 225 (4.12) nm, 280 (3.52) nm; IR (ATR)  $\nu_{max}$  3443, 3069, 1786, 1414, 1241, 1128  $cm^{-1}$ ; CD (c 0.01, MeOH) ( $\Delta\epsilon$ ) 230 (2.01), 268 (−0.98); and  $^1H$  and  $^{13}C$  NMR data (Table 4), HR-ESI-MS  $m/z$  315.1713  $[M + H]^+$  (cacl'd for  $C_{18}H_{23}N_2O_3$ ,  $m/z$  315.1703  $[M + H]^+$ ).

### 3.8. Strains and Growth Conditions for Bioactivity Test

*Candida albicans* SC5314, *C. glabrata* BG2, *C. auris* B8441, and *C. neoformans* H99 strains were grown in a 35 °C incubator and sub-cultured in yeast-extracted peptone dextrose (YPD) broth to perform the experiments.

### 3.9. Minimal Inhibitory Concentration (MIC) Assay

We conducted MIC assays to determine the efficacy of the compounds against fungal pathogens, following the EUCAST guidelines [26,27]. Overnight cultured cells were spun down and washed three times with phosphate-buffered saline (PBS), and the cell number was synchronized with an  $OD_{600}$  value of 1.0 as a fungal cell stock solution. A final 1/100 dilution in RPMI 1640 medium (#R6504; Sigma-Aldrich, St. Louis, MO, USA) was added to 96-well plates for the assay. Each compound was dissolved in dimethyl sulfoxide (DMSO) to a final concentration of 27.7 mM (1), 18.8 mM (2), 18.0 mM (3), and 16.3 mM (4) as the drug stock solution. For the assay, 5  $\mu$ L of the drug stock was inoculated into 195  $\mu$ L of the fungal cell stock solution and serially diluted into the 100  $\mu$ L of the fungal cell stock solution for 2-fold dilution. The final drug concentration for the MIC assay ranged from 5.4  $\mu$ M to 0.69 mM (1), 3.7  $\mu$ M to 0.47 mM (2), 3.5  $\mu$ M to 0.45 mM (3), and 3.2  $\mu$ M to 0.41 mM (4). The plates were incubated at 35 °C in a standing incubator for 48 h, and the  $OD_{600}$  value was detected by a microplate reader.

### 3.10. Gene Expression Analysis

*C. albicans* was treated with compounds, followed by analysis of gene expression, particularly of genes related to drug responses and virulence factors. Overnight-grown cells were inoculated into the fresh YPD broth at an  $OD_{600}$  value of 0.2 and sub-cultured to 0.8 in the early exponential growth phase. Each compound was added to the cultured broth at a 50% inhibitory concentration in Table 5, with a maximum concentration of 0.69 mM (1), 0.47 mM (2), 0.45 mM (3), and 0.41 mM (4). After 3 h of treatment, the cells were centrifuged, and total RNA was extracted using RNAiso PLUS (TaKaRa #9108) with bead beating. The extracted RNA was used as a template to synthesize cDNA, and its expression was detected using real-time quantitative PCR (TaKaRa, Kusatsu, Shiga, Japan, CronoSTAR 96 Real-Time PCR System).

### 3.11. ECD Calculation

The ground-state geometries were computed with density functional theory (DFT) calculations using Turbomole 7.7.1, the basis set def-SVP for all atoms, and the B3LYP/DFT functional level. The ground states were further confirmed using a harmonic frequency calculation. The calculated ECD data corresponding to the optimized structures were acquired with TD-DFT at the B3LYP/DFT functional level using the basis set def-TZVPP for all atoms. The CD spectra were stimulated by overlapping for each transition according to the equation below, where  $\sigma$  is the width of the band at the height of  $1/e$  and  $\Delta E_i$  and  $R_i$  are the excitation energies and rotatory strengths for transition  $i$ , respectively. In this calculation, the value of  $\sigma$  was taken to be 0.10 eV.

$$\Delta\epsilon(E) = \frac{1}{2.297 \times 10^{-39}} \frac{1}{\sqrt{2\pi\sigma}} \sum_i^A \Delta E_i R_i e^{[-(E-\Delta E_i)^2/(2\sigma)^2]}$$

**Supplementary Materials:** The following supporting information can be downloaded from <https://www.mdpi.com/article/10.3390/md22120539/s1>, Figure S1. <sup>1</sup>H NMR spectrum of 6-dimethylallyl-indole (1) at 700 MHz in CD<sub>3</sub>OD-*d*<sub>4</sub>; Figure S2. <sup>13</sup>C NMR spectrum of 6-dimethylallyl-indole (1) at 175 MHz in CD<sub>3</sub>OD-*d*<sub>4</sub>; Figure S3. COSY NMR spectrum of 6-dimethylallyl-indole (1) at 700 MHz in CD<sub>3</sub>OD-*d*<sub>4</sub>; Figure S4. HSQC NMR spectrum of 6-dimethylallyl-indole (1) at 700 MHz in CD<sub>3</sub>OD-*d*<sub>4</sub>; Figure S5. HMBC NMR spectrum of 6-dimethylallyl-indole (1) at 700 MHz in CD<sub>3</sub>OD-*d*<sub>4</sub>; Figure S6. <sup>1</sup>H NMR spectrum of 6-dimethylallyl-L-tryptophan (2) at 600 MHz in CD<sub>3</sub>OD-*d*<sub>4</sub>; Figure S7. <sup>13</sup>C NMR spectrum of 6-dimethylallyl-L-tryptophan (2) at 150 MHz in CD<sub>3</sub>OD-*d*<sub>4</sub>; Figure S8. COSY NMR spectrum of 6-dimethylallyl-L-tryptophan (2) at 600 MHz in CD<sub>3</sub>OD-*d*<sub>4</sub>; Figure S9. HSQC NMR spectrum of 6-dimethylallyl-L-tryptophan (2) at 600 MHz in CD<sub>3</sub>OD-*d*<sub>4</sub>; Figure S10. HMBC NMR spectrum of 6-dimethylallyl-L-tryptophan (2) at 600 MHz in CD<sub>3</sub>OD-*d*<sub>4</sub>; Figure S11. <sup>1</sup>H NMR spectrum of penipaline D (3) at 700 MHz in CD<sub>3</sub>OD-*d*<sub>4</sub>; Figure S12. <sup>13</sup>C NMR spectrum of penipaline D (3) at 175 MHz in CD<sub>3</sub>OD-*d*<sub>4</sub>; Figure S13. COSY NMR spectrum of penipaline D (3) at 700 MHz in CD<sub>3</sub>OD-*d*<sub>4</sub>; Figure S14. HSQC NMR spectrum of penipaline D (3) at 700 MHz in CD<sub>3</sub>OD-*d*<sub>4</sub>; Figure S15. HMBC NMR spectrum of penipaline D (3) at 700 MHz in CD<sub>3</sub>OD-*d*<sub>4</sub>; Figure S16. <sup>1</sup>H NMR spectrum of *N*-acetyl-6-dimethylallyl-L-tryptophan (4) at 900 MHz in CD<sub>3</sub>OD-*d*<sub>4</sub>; Figure S17. <sup>13</sup>C NMR spectrum of *N*-acetyl-6-dimethylallyl-L-tryptophan (4) at 225 MHz in CD<sub>3</sub>OD-*d*<sub>4</sub>; Figure S18. COSY NMR spectrum of *N*-acetyl-6-dimethylallyl-L-tryptophan (4) at 900 MHz in CD<sub>3</sub>OD-*d*<sub>4</sub>; Figure S19. HSQC NMR spectrum of *N*-acetyl-6-dimethylallyl-L-tryptophan (4) at 900 MHz in CD<sub>3</sub>OD-*d*<sub>4</sub>; Figure S20. HMBC NMR spectrum of *N*-acetyl-6-dimethylallyl-L-tryptophan (4) at 900 MHz in CD<sub>3</sub>OD-*d*<sub>4</sub>; Figure S21. HR-ESI-MS data of 6-dimethylallyl-indole (1); Figure S22. HR-ESI-MS data of 6-dimethylallyl-L-tryptophan (2); Figure S23. HR-ESI-MS data of penipaline D (3); Figure S24. HR-ESI-MS data of *N*-acetyl-6-dimethylallyl-L-tryptophan (4); Figure S25. Experimental and calculated ECD spectra of (*R*)- and (*S*)-6-dimethylallyl-L-tryptophan (2); Figure S26. Experimental and calculated ECD spectra of (*R*)- and (*S*)-*N*-Acetyl-6-dimethylallyl-L-tryptophan (4); Table S1. ECD calculation of (*R*)- 6-dimethylallyl-L-tryptophan (2); Table S2. ECD calculation of (*S*)-6-dimethylallyl-L-tryptophan (2); Table S3. ECD calculation of (*R*)-*N*-Acetyl-6-dimethylallyl-L-tryptophan (4); Table S4. ECD calculation of (*S*)-*N*-Acetyl-6-dimethylallyl-L-tryptophan (4); Table S5. Cartesian coordinates of (*R*)-6-dimethylallyl-L-tryptophan (2); Table S6. Cartesian coordinates of (*S*)- 6-dimethylallyl-L-tryptophan (2); Table S7. Cartesian coordinates of (*R*)-*N*-Acetyl-6-dimethylallyl-L-tryptophan (4); Table S8. Cartesian coordinates of (*S*)-*N*-Acetyl-6-dimethylallyl-L-tryptophan (4).

**Author Contributions:** S.U.: data curation, formal analysis, visualization, writing—original draft, review and editing. H.J.: data curation, formal analysis, visualization, writing—original draft. J.-E.P.: data curation, formal analysis, writing—original draft. J.S.: data curation, formal analysis. S.H.J.: data curation, formal analysis. M.B.: data curation, formal analysis, writing—original draft. K.-T.L.: conceptualization, resources, supervision, funding acquisition, writing—original draft, review and editing, visualization. K.M.: conceptualization, resources, supervision, funding acquisition, writing—original draft, review and editing, visualization. All authors have read and agreed to the published version of the manuscript.

**Funding:** This work was supported by National Research Foundation of Korea (NRF) grants funded by the Korean government (MSIT) (2021R1C1C1009609 to K. Moon and 2022R1C1C2003274, 2021R1A6C101C369 to K.-T.L.; 2022R1A4A3022401 to K.-T.L. and K.M.) and the Korea Basic Science Institute under the R&D program (Project No. C230430 to K. Moon.) and supervised by the Ministry of Science and ICT. This research was partially supported by the “Regional Innovation Strategy (RIS)” through the National Research Foundation of Korea (NRF), funded by the Ministry of Education (MOE) (2023-RIS-008 to K.-T.L.).

**Institutional Review Board Statement:** Not applicable.

**Data Availability Statement:** The original data presented in the study are included in the article/Supplementary Material; further inquiries can be directed to the corresponding author.

**Conflicts of Interest:** The authors declare no conflict of interest.

## References

1. Zeleke, J.; Lu, S.-L.; Wang, J.-G.; Huang, J.-X.; Li, B.; Ogram, A.V.; Quan, Z.-X. Methyl coenzyme M reductase A (*mcrA*) gene-based investigation of methanogens in the mudflat sediments of Yangtze River Estuary, China. *Microb. Ecol.* **2013**, *66*, 257–267. [[CrossRef](#)]
2. Böer, S.I.; Hedtkamp, S.I.C.; van Beusekom, J.E.E.; Fuhrman, J.A.; Boetius, A.; Ramette, A. Time- and sediment depth-related variations in bacterial diversity and community structure in subtidal sands. *ISME J.* **2009**, *3*, 780–791. [[CrossRef](#)]
3. Lv, X.; Ma, B.; Yu, J.; Chang, S.X.; Xu, J.; Li, Y.; Wang, G.; Han, G.; Bo, G.; Chu, X. Bacterial community structure and function shift along a successional series of tidal flats in the Yellow River Delta. *Sci. Rep.* **2016**, *6*, 36550. [[CrossRef](#)]
4. Ryu, D.; Hillman, P.F.; Akinniyi, G.; Nam, S.-J.; Yang, I. Marine mudflat actinomycetes as a novel natural products source. *Front. Mar. Sci.* **2023**, *10*, 1297446. [[CrossRef](#)]
5. Sivalingam, P.; Hong, K.; Pote, J.; Prabakar, K. Extreme environment *Streptomyces*: Potential sources for new antibacterial and anticancer drug leads? *Int. J. Microbiol.* **2019**, *2019*, 5283948. [[CrossRef](#)]
6. Seo, J.; Shin, Y.-H.; Jo, S.J.; Du, Y.E.; Um, S.; Kim, Y.R.; Moon, K. Cystargamides C and D, new cyclic lipopeptides from a tidal mudflat-derived *Streptomyces* sp. JMS132. *Front. Microbiol.* **2022**, *13*, 904954. [[CrossRef](#)]
7. Jeong, H.; Jo, S.J.; Bae, M.; Kim, Y.R.; Moon, K. Actinoflavosides B–D, flavonoid type glycosides from tidal mudflat-derived actinomycetes. *Mar. Drugs* **2022**, *20*, 565. [[CrossRef](#)]
8. Weber, J.M.; Wierman, C.K.; Hutchinson, C.R. Genetic analysis of erythromycin production in *Streptomyces erythreus*. *J. Bacteriol.* **1985**, *164*, 425–433. [[CrossRef](#)]
9. Darken, M.A.; Berenson, H.; Shirk, R.J.; Sjolander, N.O. Production of tetracycline by *Streptomyces aureofaciens* in synthetic media. *Appl. Microbiol.* **1960**, *8*, 46–51. [[CrossRef](#)]
10. Johnstone, D.B.; Waksman, S.A. Streptomycin II, an antibiotic substance produced by a new species of *Streptomyces*. *Proc. Soc. Exp. Biol. Med.* **1947**, *65*, 294–295. [[CrossRef](#)]
11. Brautaset, T.; Sekurova, O.N.; Sletta, H.; Ellingsen, T.E.; StrŁm, A.R.; Valla, S.; Zotchev, S.B. Biosynthesis of the polyene antifungal antibiotic nystatin in *Streptomyces noursei* ATCC 11455: Analysis of the gene cluster and deduction of the biosynthetic pathway. *Chem. Biol.* **2000**, *7*, 395–403. [[CrossRef](#)]
12. Lomovskaya, N.; Otten, S.L.; Doi-Katayama, Y.; Fonstein, L.; Liu, X.C.; Takatsu, T.; Inventi-Solari, A.; Filippini, S.; Torti, F.; Colombo, A.L.; et al. Doxorubicin overproduction in *Streptomyces peuceitius*: Cloning and characterization of the *dnrU* ketoreductase and *dnrV* genes and the *doxA* cytochrome P-450 hydroxylase gene. *J. Bacteriol.* **1999**, *181*, 305–318. [[CrossRef](#)]
13. Yim, C.-Y.; Le, T.C.; Lee, T.G.; Yang, I.; Choi, H.; Lee, J.; Kang, K.-Y.; Lee, J.S.; Lim, K.-M.; Yee, S.-T.; et al. Saccharomonopyrones A–C, new  $\alpha$ -pyrones from a marine sediment-derived bacterium *Saccharomonospora* sp. CNQ-490. *Mar. Drugs* **2017**, *15*, 239. [[CrossRef](#)]
14. Le, T.C.; Katila, N.; Park, S.; Lee, J.; Yang, I.; Choi, H.; Choi, D.Y.; Nam, S.J. Two new secondary metabolites, saccharochlorines A and B, from a marine bacterium *Saccharomonospora* sp. KCTC-19160. *Bioorg. Med. Chem. Lett.* **2020**, *30*, 127145. [[CrossRef](#)]
15. Li, M.-Y.; Xiao, Q.; Pan, J.-Y.; Wu, J. Natural products from semi-mangrove flora: Source, chemistry and bioactivities. *Nat. Prod. Rep.* **2009**, *26*, 281–298. [[CrossRef](#)]
16. Muwawa, E.M.; Obieze, C.C.; Makonde, H.M.; Jefwa, J.M.; Kahindi, J.H.P.; Khasa, D.P. 16S rRNA gene amplicon-based metagenomic analysis of bacterial communities in the rhizospheres of selected mangrove species from Mida Creek and Gazi Bay, Kenya. *PLoS ONE* **2021**, *16*, e0248485. [[CrossRef](#)]
17. Turaev, D.; Rattei, T. High definition for systems biology of microbial communities: Metagenomics gets genome-centric and strain-resolved. *Curr. Opin. Biotechnol.* **2016**, *39*, 174–181.
18. Ye, Y.-L.; Ma, K.-J.; Fu, Y.-H.; Wu, Z.-C.; Fu, G.-Y.; Sun, C.; Xu, X.-W. The heterogeneity of microbial diversity and its drivers in two types of sediments from tidal flats in Beibu Gulf, China. *Front. Mar. Sci.* **2023**, *10*, 1256393. [[CrossRef](#)]
19. Takahashi, S.; Takagi, H.; Toyoda, A.; Uramoto, M.; Nogawa, T.; Ueki, M.; Sakaki, Y.; Osada, H. Biochemical characterization of a novel indole prenyltransferase from *Streptomyces* sp. SN-593. *J. Bacteriol.* **2010**, *192*, 2839–2851. [[CrossRef](#)]
20. Satou, R.; Izumikawa, M.; Katsuyama, Y.; Matsui, M.; Takagi, M.; Shin-ya, K.; Ohnishi, Y. Isolation, structural elucidation and biosynthesis of 3-hydroxy-6-dimethylallylindolin-2-one, a novel prenylated indole derivative from *Actinoplanes missouriensis*. *J. Antibiot.* **2014**, *67*, 231–236. [[CrossRef](#)]
21. Sasaki, T.; Igarashi, Y.; Ogawa, M.; Furumai, T. Identification of 6-prenylindole as an antifungal metabolite of *Streptomyces* sp. TP-A0595 and synthesis and bioactivity of 6-substituted indoles. *J. Antibiot.* **2002**, *55*, 1009–1012. [[CrossRef](#)] [[PubMed](#)]
22. Li, C.-S.; Li, X.-M.; An, C.-Y.; Wang, B.-G. Prenylated indole alkaloid derivatives from marine sediment-derived fungus *Penicillium paneum* SD-44. *Helv. Chim. Acta* **2014**, *97*, 1440–1444. [[CrossRef](#)]
23. Arendrup, M.C.; Patterson, T.F. Multidrug-resistant *Candida*: Epidemiology, molecular mechanisms, and treatment. *J. Infect. Dis.* **2017**, *216*, S445–S451. [[CrossRef](#)]
24. Bartram, A.K.; Lynch, M.D.; Stearns, J.C.; Moreno-Hagelsieb, G.; Neufeld, J.D. Generation of multimillion-sequence 16S rRNA gene libraries from complex microbial communities by assembling paired-end illumina reads. *Appl. Environ. Microbiol.* **2011**, *77*, 3846–3852. [[CrossRef](#)]
25. Yarza, P.; Yilmaz, P.; Pruesse, E.; Glöckner, F.O.; Ludwig, W.; Schleifer, K.-H.; Whitman, W.B.; Euzéby, J.; Amann, R.; Rosselló-Móra, R. Uniting the classification of cultured and uncultured bacteria and archaea using 16S rRNA gene sequences. *Nat. Rev. Microbiol.* **2014**, *12*, 635–645. [[CrossRef](#)]

- 
26. Berkow, E.L.; Lockhart, S.R.; Ostrosky-Zeichner, L. Antifungal susceptibility testing: Current approaches. *Mar. Drugs* **2020**, *33*, e00069-19. [[CrossRef](#)]
  27. Choi, J.W.; Lee, K.T.; Kim, S.; Lee, Y.R.; Kim, H.J.; Seo, K.J.; Lee, M.H.; Yeon, S.K.; Jang, B.K.; Park, S.J.; et al. Optimization and evaluation of novel antifungal agents for the treatment of fungal infection. *J. Med. Chem.* **2021**, *64*, 15912–15935. [[CrossRef](#)]

**Disclaimer/Publisher’s Note:** The statements, opinions and data contained in all publications are solely those of the individual author(s) and contributor(s) and not of MDPI and/or the editor(s). MDPI and/or the editor(s) disclaim responsibility for any injury to people or property resulting from any ideas, methods, instructions or products referred to in the content.